JOURNAL OF MATERIALS SCIENCE **36** (2001) 313–319

Oxidation behavior of hot-pressed $MoSi_2$-TiC composite

Q. ZHU, K. SHOBU, Y. ZENG, T. WATANABE
Kyushu National Industrial Research Institute, 841-0052, Japan
E-mail: qszhu@hotmail.com

The oxidation behavior of a hot-pressed $MoSi_2$-TiC composite was investigated in air over the temperature range of 500 °C–1400 °C. The composite exhibits parabolic oxidation kinetics between 500 °C–800 °C, where the activation energy was calculated to be 32 kJ/mol. However, above 800 °C, it shows two-step parabolic oxidation kinetics, where the first stage (step I) was proposed to be dominated by the oxidation of surface TiC particles. After all the surface TiC particles are oxidized, the oxidation of the composite turns into the second stage (step II) which was controlled by the oxidation of $MoSi_2$. The activation energy was determined to be 130 kJ/mol and 141 kJ/mol for step I and step II, respectively. A dense cristobalite scale with TiO_2 in lath shapes on the top was observed after oxidation at 1400 °C.

1. Introduction

Molybdenum silicide ($MoSi_2$) has been proposed as a promising intermetallic compound for high temperature structural applications due to its high melting-point (∼2020 °C), excellent high-temperature oxidation resistance and brittle-to-ductile transition (BDT) above ∼1000 °C [1–4]. Above the BDT temperature (BDTT), the failure behavior of $MoSi_2$ becomes more predictable, and it could be processed via conventional metallurgical processing like hot deformation. However, due to the same property, the strength of $MoSi_2$ decreases with increasing temperature above the BDTT. Moreover, $MoSi_2$ exhibits a low fracture toughness at ambient temperature [5]. Therefore, it is necessary to toughen the material at low temperature (below the BDTT) while simultaneously improving the strength at high temperature (above the BDTT) before $MoSi_2$ could be used in high-temperature structural applications. These two goals can be accomplished by alloying with other silicides or by compositing with particulates or whisker reinforcement [1]. Much effort has thus been made to reinforce $MoSi_2$ with SiC particulates or whiskers [1, 6–9]. TiC is another potential reinforcement for $MoSi_2$ as (1) TiC was reported to have a brittle-to-ductile transition above 600 °C [10]; (2) the thermal expansion coefficient of TiC is nearly the same as that of $MoSi_2$ [10]; and (3) TiC is chemically compatible with $MoSi_2$ at least up to 1600 °C [1, 2, 10]. The $MoSi_2$-TiC composites have been fabricated through the hot pressing (HP) process [11, 12] as well as the self-propagation high-temperature synthesis (SHS) technique [13]. Yang *et al*. [11, 12] reported a decrease in the fracture strength on hot-pressed $MoSi_2$-20 vol% TiC composites compared with that of monolithic $MoSi_2$, where the decrease was attributed to the nonuniform distribution of the TiC reinforcement. In another study, a significant increase in the fracture toughness (from 2.11 to 9.82 MPa·$m^{1/2}$) was demonstrated by Pho *et al*. [14] on a hot-pressed $MoSi_2$-20 vol% TiC composite, which is in agreement with our preliminary studies concerning the mechanical properties of the $MoSi_2$-TiC composite. Despite the fact that TiC has a great potential to reinforce $MoSi_2$ through further optimizing the microstructure and composition, the high-temperature oxidation resistance of the composite is one of the major concerns because TiC exhibits poor high-temperature oxidation resistance compared with that of $MoSi_2$ [15]. Up to now, detailed studies on the oxidation behavior of the $MoSi_2$-TiC composite have not yet been reported in the literature.

The main objective of the present study is to investigate the oxidation behavior of a hot-pressed $MoSi_2$-TiC composite with some attention to the oxidation thermodynamics of this system.

2. Experimental procedure

2.1. Sample preparation

The $MoSi_2$-TiC composite was synthesized through hot-pressing from the raw powders of $MoSi_2$ (6 μm, Japan New Metals) and TiC (1.1 μm, Japan New Metals). The $MoSi_2$ powder was first wet-ball milled in alcohol for 72 h, and then the milled $MoSi_2$ was mixed with the TiC powder to form a powder mixture with a $MoSi_2$-20 wt% TiC composition, followed by dry ball-milling for 24 h. Free carbon up to several percent was also added to the mixture as the deoxidant to remove the SiO_2 phases during HP. The mixture was then packed into a graphite die, followed by hot-pressing under an applied pressure of 25 MPa at 1400 °C–1700 °C for 0.5–2 h. The resultant disks were 12 mm in diameter and about 6 mm in thickness. Approximately 1 mm was ground out from each surface of the disk to eliminate the

region possibly affected by the graphite die. The room-temperature fracture strength was measured by a three-point bending fixture with an outer span of 10 mm under a crosshead speed of 0.5 mm/min in air. Specimens for this test were cut and ground into rectangle bars with nominal dimensions of 4 mm × 2 mm × 12 mm.

The microstructure of the $MoSi_2$-TiC composite was characterized using an optical microscopy and a scanning electron microscopy (SEM). An energy-dispersive X-ray spectrometer (EDS) was used to determine the composition of the composite. The crystalline phases were evaluated using an X-ray diffractometer (XRD). The density of the samples was determined by Archimedes' principle using water.

2.2. Oxidation tests

Oxidation tests were performed under natural convection conditions in air from 500 °C to 1400 °C for 100 h using a thermogravimetric analyzer (DT-300, Shimatsu Corp., Japan). The sensitivity of this system could reach 0.001 mg, and the accuracy of 0.01 mg was commonly used in the present study. The furnace of this system was changed to heat by tubular silicon carbide to achieve testing temperatures above 1300 °C. Oxidation specimens were cut from the disk and ground to the nominal dimensions of 4 mm × 3 mm × 2 mm, followed by polishing in successive steps to 1 μm. They were then ultrasonically cleaned in acetone and water, and dried at 110 °C for 2 h before the oxidation tests. The specimen was supported by a high-purity alumina crucible. The temperature of the specimen was then increased to the designated temperature at the rate of 20 °C/min and held for 100 h, followed by cooling to 400 °C at the rate of 20 °C/min. The mass change and temperature were continuously recorded by a personnel computer. After oxidation, the samples were characterized with respect to microstructure and scale composition using the SEM/EDS and XRD.

3. Results and discussion

3.1. Composite synthesis

It is relatively easy to densify the $MoSi_2$-TiC composite by HP under 25 MPa. For example, a one-hour HP at 1600 °C is sufficient to obtain composites with a relative density greater than 98%. However, investigations revealed that the composite contained many spherical SiO_2 phases that resulted from the slight oxidation of the $MoSi_2$ raw powder. Therefore, free carbon was added to remove the SiO_2 phases, and several percent proved to be sufficient to remove the SiO_2 phases. Fig. 1 shows a typical XRD pattern of the composite with 1 wt% carbon addition. All peaks fit very well with the tetragonal $MoSi_2$ (PDF 41-0612) and cubic TiC (PDF 71-0298). The typical microstructure of the composite is shown in Fig. 2, together with the

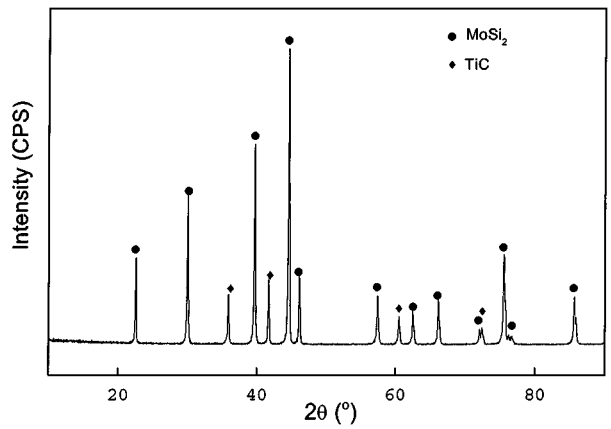

Figure 1 Typical XRD pattern of the $MoSi_2$-20 wt% TiC-1 wt% C composite.

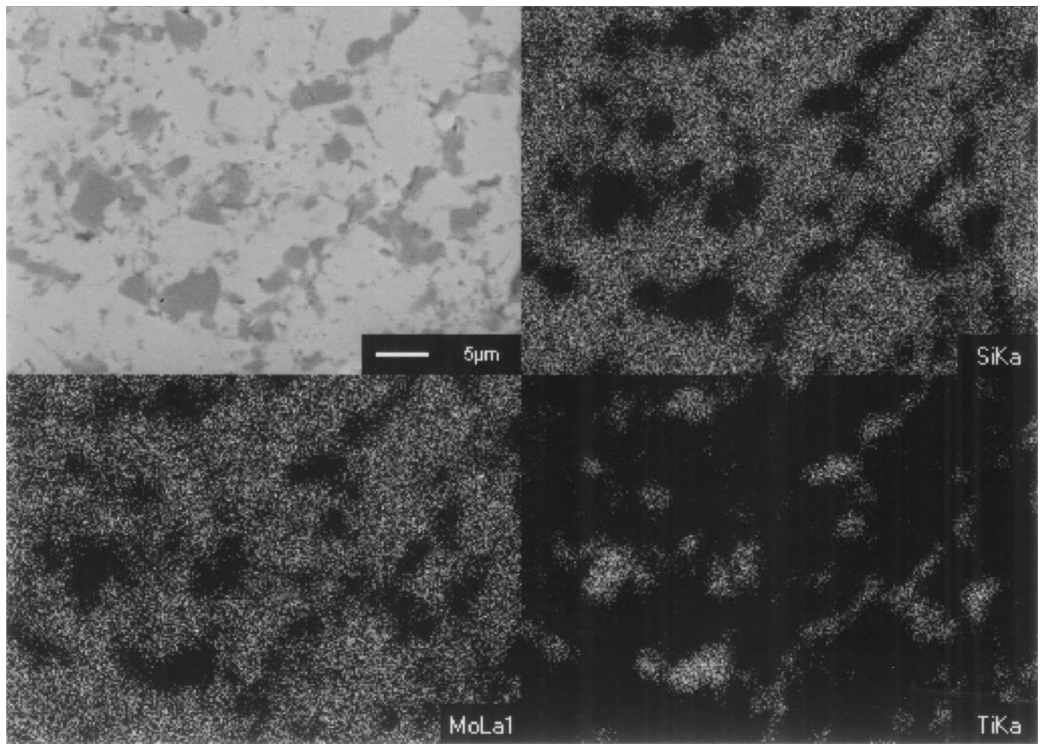

Figure 2 Typical microstructure of the $MoSi_2$-20 wt% TiC-1 wt%C composite. The composite was hot-pressed at 1600 °C for 1 h. As indicated by the elemental distribution map, the dark phases are TiC phases, and the grey phases are $MoSi_2$ phases.

TABLE I Fracture strength of the $MoSi_2$-TiC composite

Material	Monolithic $MoSi_2$	$MoSi_2$-20 wt% TiC (no carbon addition)	$MoSi_2$-20 wt% TiC (1 wt% carbon addition)
Fracture strength (MPa)	335	481	689

elemental distribution of Si, Mo and Ti. The dark phases are TiC phases and the gray phases are the $MoSi_2$ matrix. No other phases were detected by the SEM/EDS. These investigations confirmed that the composite is only composed of $MoSi_2$ and TiC phases, although some grain-boundary SiO_2 phases may exist and can not be detected by the SEM/EDS and XRD investigations.

The room-temperature fracture strength of the composite was determined to be 681 MPa as listed in Table I. The strength of the monolithic $MoSi_2$ and $MoSi_2$-TiC without carbon addition is also included in Table I for comparison. It shows that $MoSi_2$ is significantly strengthened by the TiC particles and a further strengthening effect is achieved after removing the silica phases from the composite through carbon addition. This is in good agreement with the results reported by Maloy *et al*. [8], where the $MoSi_2$ was found to be toughened by 2 wt% carbon addition, which was attributed to the absence of SiO_2 phases and the presence of SiC and Mo_5Si_3C phases. The strengthening effects in the present study may be mainly due to the absence of the SiO_2 phases as SiC, Mo_5Si_3C and other phases were not detected after the carbon addition.

3.2. Thermodynamics of the Mo-Ti-Si-O-C system

The objectives of this study are to investigate the chemical compatibility among various phases at elevated temperatures and to elucidate the phase changes during the oxidation process. The thermodynamic study was based on minimizing the free energy [16] as indicated by equations 1 and 2.

$$\text{Min: } G = \sum_{j=1}^{M} \sum_{i=1}^{N_j} n_i \mu_i \qquad (1)$$

$$\text{Conservation of Mass: } \sum_{k=1}^{M} \sum_{i=1}^{N_k} a_{ij} n_i = B_j \quad (j = 1, 2, \ldots, N) \qquad (2)$$

where G is the total free energy of the system, M is the total phases in the system, n_i is the molar quantity of the ith substance in a specified phase, N_j is the total number of substances in the jth phase, μ_i is the chemical potential of the ith substance under the specified condition, N is the number of elements in the system, a_{ij} is the molar quantity of the jth element in the ith substance in a specified phase and B_j is the total molar quantity of the jth element in the system. The thermodynamic simulation was performed using previously developed software [17]. The following substances are included in the thermodynamic simulation, namely, the gas phases: air (N_2 and O_2), CO, CO_2, SiO(g), MoO_2(g), MoO_3(g), TiO(g) and TiO_2(g); liquid phase: MoO_3(l); and solid phases: Mo_5Si_3, $MoSi_2$, Mo_3Si, MoC, MO_2C, SiC, TiC, Ti_5Si_3, TiSi, $TiSi_2$, Mo, Ti, C (graphite), Si, SiO_2, MoO_2, MoO_3, Mo_4O_{11}, Mo_8O_{23}, Mo_9O_{26}, TiO, TiO_2 (rutile), TiO_2 (anatase), Ti_2O_3, Ti_3O_5 and Ti_4O_7. All thermodynamic data are taken from references [18, 19]. The chemical compatibility between $MoSi_2$ and TiC, the interface stability of TiC/SiO_2 and $MoSi_2$/TiO_2 and the phase changes during oxidation were studied up to 2000 K. It is reported that atomic oxygen can replace the carbon to form the oxycarbide, TiC_xO_{1-x}($x < 0.5$) [20], the TiC_xO_{1-x} is not considered in the present simulation due to the lack of thermodynamic data.

3.2.1. Chemical compatibility between $MoSi_2$ and TiC

The calculations revealed that $MoSi_2$ is chemically compatible with TiC to at least 2000 K, consistent with the previously reported experimental and simulated results [1, 2] Pho et al. [14] reported that SiC and Mo_5Si_3 appeared after hot-pressing on a $MoSi_2$-5 wt% TiC composite. This discrepancy is attributed to the slight oxidation of the $MoSi_2$ raw powder, where according to the thermodynamic calculation, small amount of SiC and Mo_5Si_3 will appear if the system initially contains small amount of SiO_2. The thermodynamic calculations also predicted that the SiC and Mo_5Si_3 phases appeared when carbon was used as the deoxidant to remove the SiO_2 phases, which is inconsistent with the experimental results of Maloy *et al*. [8], where the Mo_5Si_3C (also known as the Nowotny phase) and SiC were actually formed (the $MoSi_2$ is the main phase). It should be noted that the Mo_5Si_3C phase was not included in this simulation due to the lack of accurate free energy data of this phase. Therefore, this calculation can not exclude the existence of the Mo_5Si_3C phase.

3.2.2. Interface stability of TiC/SiO_2 and $MoSi_2$/TiO_2

Several kinds of interfaces may appear after oxidation of the composite. Among them, the SiO_2/$MoSi_2$ and the TiO_2/TiC interfaces would be thermodynamically stable. The calculations showed that the TiC/SiO_2 interface is also thermodynamically stable during oxidation, which implies that the SiC/TiO_2 interface is not thermodynamically stable and tends to react to form SiO_2 and TiC as indicated by reaction (3). However, the $MoSi_2$/TiO_2 interface was predicted to be unstable based on the thermodynamic simulation. $MoSi_2$ would react with TiO_2 according to reaction (4), where for example, at 1400 K the free energy of the left side and right side is −808.229 kJ and −842.279 kJ, respectively.

$$SiC + TiO_2 = SiO_2 + TiC \qquad (3)$$

$$MoSi_2 + TiO_2 = 0.25SiO_2 + 0.5Ti_2O_3 + 0.8215MoSi_2 + 0.0357Mo_5Si_3 \qquad (4)$$

3.2.3. Oxidation thermodynamics of the $MoSi_2$-TiC composite

It is well known that the oxidation behavior of silicide is sensitive to the oxidation environment (oxygen partial pressure, etc.). Such dependence is also manifested in the $MoSi_2$-TiC composite. If there is sufficient oxygen during the oxidation, the oxidation behavior of the composite is quite simple, e.g., every substance will be oxidized to the most stable oxide like CO_2, SiO_2 and TiO_2 (rutile) as indicated by reactions (5) and (6).

$$MoSi_2 + 3.5O_2 = MoO_3 + 2SiO_2 \quad (5)$$

$$TiC + 2O_2 = TiO_2\,(\text{rutile}) + CO_2 \quad (6)$$

However, if the oxygen is insufficient in the system, the oxidation behavior of the composite becomes complicated. It generally shows the selective oxidation of silicon on the $MoSi_2$ phases as shown by reactions (7) and (8). The reaction that would take priority depends on the oxidation conditions and could be determined through the thermodynamic simulation. On the other hand, it tends to form Ti_2O_3 on the TiC constituent as expressed by reaction (9). Unlike the $MoSi_2$, the formation of metallic titanium is not thermodynamically preferred in oxygen lean environments. Thermodynamic simulations also predict that Mo_2C phase may form together with Mo_5Si_3 or Mo under certain circumstances.

$$5MoSi_2 + 7O_2 = Mo_5Si_3 + 7SiO_2 \quad (7)$$

$$MoSi_2 + 2O_2 = Mo + 2SiO_2 \quad (8)$$

$$2TiC + 2.5O_2 = Ti_2O_3 + 2CO \quad (9)$$

As previously reported [21], the further oxidation of Mo_5Si_3 can be expressed by reactions (10) and (11), depending on the oxidation atmosphere. Reaction (10) is preferred in an excessive oxygen environment, while the preferential oxidation of silicon occurs in an oxygen-lean environment as indicated by reaction (11).

$$2Mo_5Si_3 + 21O_2 = 10MoO_3 + 6SiO_2 \quad (10)$$

$$Mo_5Si_3 + 3O_2 = 5Mo + 3SiO_2 \quad (11)$$

3.3. Oxidation behavior

The oxidation-induced isothermal mass-changes are illustrated in Fig. 3. The oxidation behavior of the composite generally follows a parabolic law. Weight gain was observed in all temperatures investigated. As previously stated, the oxidation of the composite in excessive oxygen environments proceeds according to reactions (5) and (6), where reaction (5) predicts a net weight-gain of 74% if the MoO_3 does not evaporate at all, whereas it is a net weight-loss of 21% if the MoO_3 totally evaporates. The oxidation of TiC will generate a net weight-gain of 33%. The competition of the weight-loss and weight-gain reactions determines the weight change behavior during the oxidation. The oxide scale below 800 °C would be a mixture of SiO_2, TiO_2 and MoO_3. As exhibited by the SEM photograph in Fig. 4a,

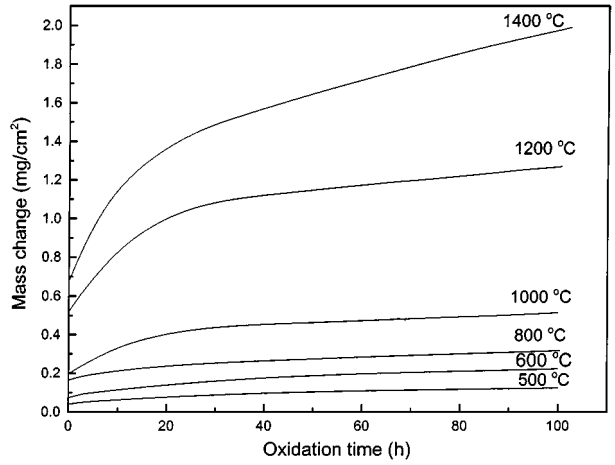

Figure 3 Oxidation-induced mass changes of the $MoSi_2$-TiC composite as a function of oxidation time in air at 500 °C–1400 °C.

the oxide scale at 500 °C shows two distinct areas, mirroring the makeup of the composite. Bright phases are TiO_2 phases that resulted from the oxidation of surface TiC particles, while the grey phases are $MoSi_2$ phases covered by an oxidation-induced mixture of SiO_2 and MoO_3. The absence of MoO_3 peaks in the XRD pattern combined with the fact that MoO_3 whiskers that are commonly observed during the oxidation of $MoSi_2$ and other silicides [22, 23] were not found, suggests that MoO_3 formed is amorphous. Pest disintegration of $MoSi_2$ was not observed at 500 °C possibly due to the limited oxidation time (100 h) as pest disintegration needs a long nucleation (incubation) period [23], or due to the high-density of the composite because a recent study of the low-temperature oxidation of $MoSi_2$ revealed that pest did not occur in dense (>95%) $MoSi_2$ for exposure times up to 588 h [24]. The oxide scale at 600 °C and 800 °C is similar to that at 500 °C as exhibited by Fig. 4b and c. The growth of TiO_2 is attributed to the oxidation-induced volume expansion of the TiC phases, where according to reaction (6), the oxidation of TiC will generate a volume expansion of 54%. The XRD pattern in Fig. 5 indicates that the TiO_2 formed at these temperatures is rutile. The oxide scales at 1000 °C–1400 °C consist of an outer rutile layer and an inner silica layer as shown in Fig. 4d to f. Fig. 4f demonstrates a dense cristobalite scale with TiO_2 in a lath shape on the top after oxidation for 100 h at 1400 °C. The micro-cracks on the oxide film have been attributed to the thermal stress that resulted from thermal expansion differences between the substrate and the silica layer [25]. The dense silica film is a good barrier to oxygen diffusion, providing good oxidation resistance for the composite at high temperature.

The weight change behavior of the composite is correlated to the parabolic law by the following equation.

$$R^2 = k_p t \quad (12)$$

where R is the oxidation rate in mg/cm^2 and k_p is the parabolic rate constant. The calculated $R^2 - t$ curves are shown in Fig. 6. It shows that the R^2 vs. t curves are linear up to 800 °C, whereas at 1000 °C and above, it shows a "two-step parabolic oxidation," suggesting

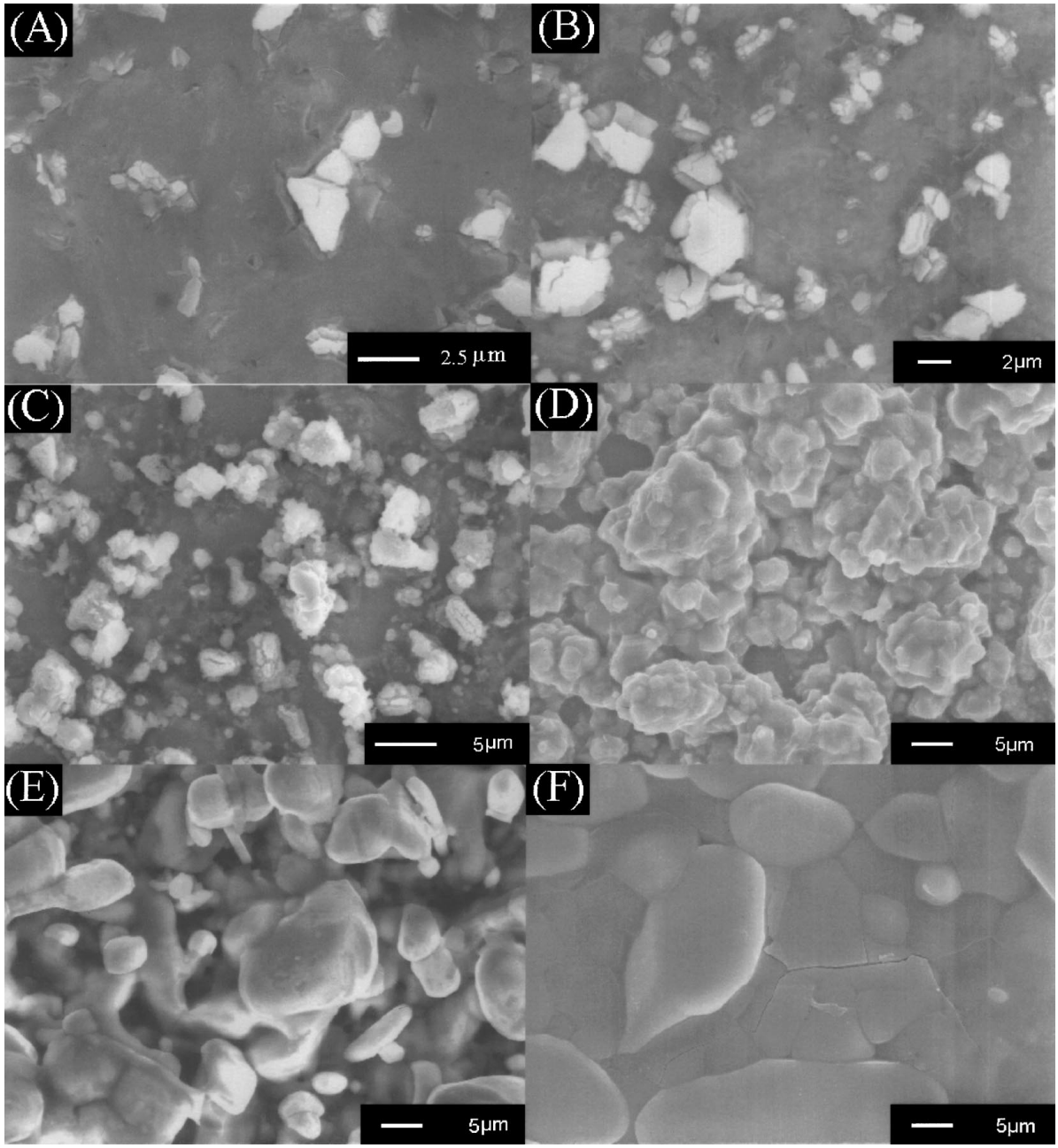

Figure 4 SEM micrographs of oxide scales formed on the $MoSi_2$-TiC composite after oxidation in air at: (a) 500 °C , (b) 600 °C, (c) 800 °C, (d) 1000 °C, (e)1200 °C, and (f)1400 °C.

a change in the oxidation mechanism at these temperatures. The parabolic rate constant k_p was determined from the slope of the $R^2 - t$ curves in Fig. 6 and plotted as $lnk_p \sim 1/T$ in Fig. 7 for determining the activation energy. The activation energy at 500 °C–800 °C was calculated to be 32 kJ/mol. This is in good agreement with the activation energy values of 42–71 kJ/mol reported for the oxidation of TiC at 420 °C–500 °C by Shimada *et al*. [26], suggesting that at 500–800 °C the oxidation of the composite was dominated by the oxidation of the surface TiC particles. As indicated by the XRD patterns in Fig. 5, the surface TiC particles are not totally oxidized even after 100 h oxidation at 500–800 °C, so the $R^2 - t$ curves only manifest one linear stage. However, the oxidation rate of TiC increases with increasing temperature. At 1000 °C and above, the surface TiC particles could be totally oxidized within a short time. After all the surface TiC particles are oxidized, the oxidation of the composite would be controlled by the oxidation of the $MoSi_2$ phases, which results in the "two-step" oxidation behavior, where step I is mainly dominated by the oxidation of the surface TiC particles. This point can be confirmed by comparing the oxidation activation energy with that in the literature. The activation energy for step I was determined to be 130 kJ/mol, which is in reasonable agreement with the value of 190 kJ/mol reported for the oxidation of the Al_2O_3-30 vol% TiC composite at 900 °C–1100 °C, where the rate limiting step was assumed to be the diffusion of oxygen through the TiO_2 layer [27]. The activation energy for step II was determined to be 141 kJ/mol, which is in good agreement with the values of 113–121 kJ/mol reported for the oxygen diffusion over vitreous silica film [28–30],

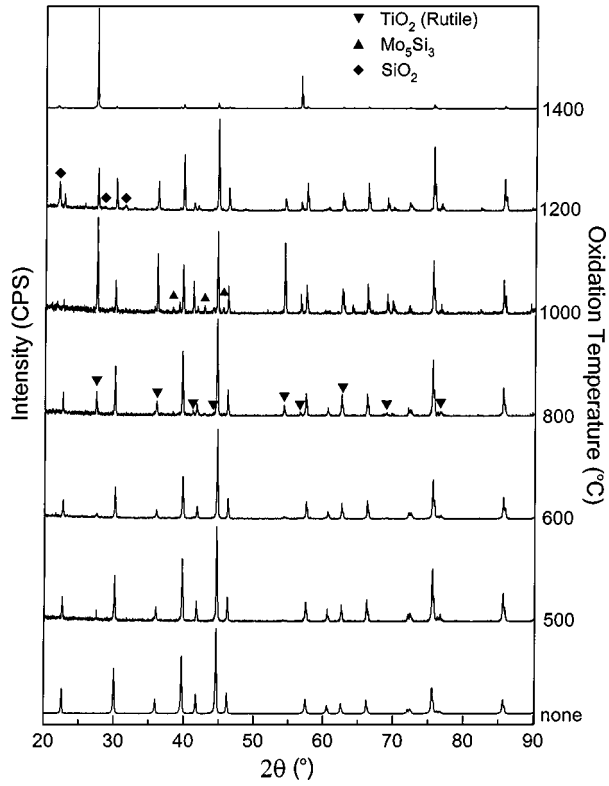

Figure 5 XRD patterns of the oxidized surfaces of the $MoSi_2$-TiC composite after oxidation at 500 °C–1400 °C in air for 100 h.

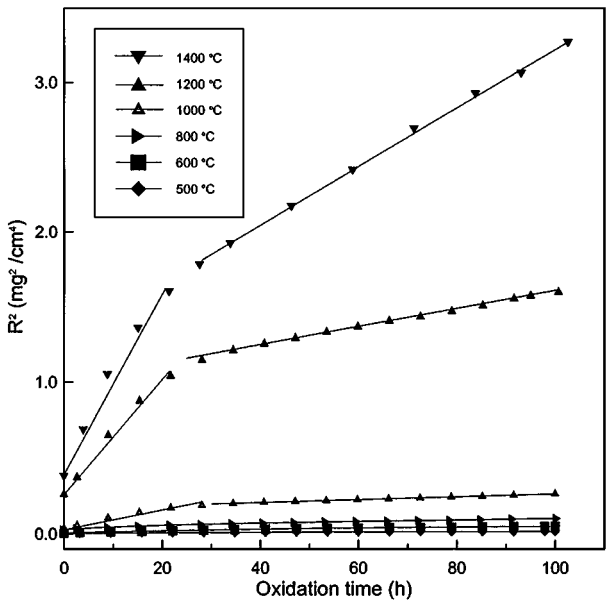

Figure 6 Parabolic plots of weight gain for oxidation of the $MoSi_2$-TiC composite.

and the value of 112 kJ/mol calculated from the oxidation data reported for the $MoSi_2$-SiC composite at 1300 °C and 1400 °C in air [31].

The thermodynamic studies are in reasonable agreement with the experimental data, which revealed the formation of Mo_5Si_3 between 800 °C and 1200 °C. During the initial oxygen period, the composite would be fully oxidized to SiO_2, TiO_2 and MoO_3 because there is sufficient oxygen. However, after an oxide scale (porous or dense) forms, further oxidation could only proceed via the diffusion of reactants and oxidation

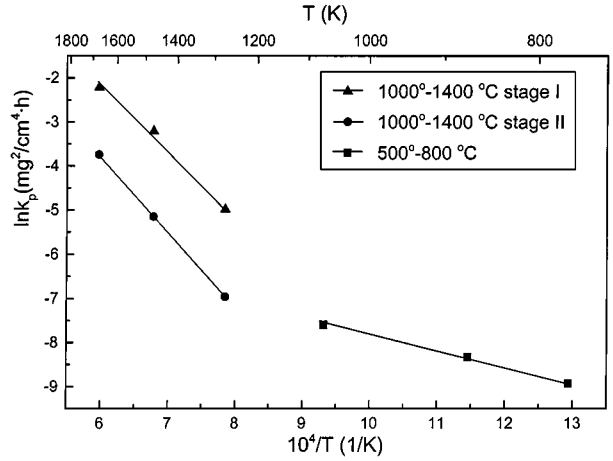

Figure 7 Arrhenius plots of parabolic rate constant (k_p) for oxidation of the $MoSi_2$-TiC composite.

products through the oxide scale. The overall oxidation rate may be limited by the diffusion of oxygen through the gas boundary layer and the oxide scale, or by the governing reaction, or by the diffusion of oxidation products out through the oxide scale and the gas boundary layer. If the oxidation is limited by the governing reaction or by the transfer of the oxidation products, the partial pressure of oxygen must be higher than the equilibrium partial pressure at the interface of the oxide scale and the substrate, therefore, selective oxidation will not occur. A molybdenum-rich (Mo_5Si_3) interlayer was actually formed, indicating that oxygen transportation is the rate-limiting step. This combined with the activation energy of 141 kJ/mol may suggest that the rate-limiting step is the oxygen diffusion through the oxide scale.

4. Conclusions

The $MoSi_2$-TiC composite was fabricated by HP under 25 MPa. Free carbon was added to remove the SiO_2 phases during the HP. Preliminary investigations showed that $MoSi_2$ could be significantly strengthened through compositing with TiC.

The thermodynamic study shows that $MoSi_2$ and TiC are chemically compatible up to at least 2000 K. It also revealed that the oxidation of the composite in oxygen lean environments is complicated, and reactions for the selective oxidation of silicon and the formation of Ti_2O_3 are thermodynamically preferred under such conditions.

The oxidation behavior of the composite was tested in air over the temperature range of 500 °C–1400 °C. Parabolic oxidation kinetics were observed between 500 °C–800 °C, where the activation energy was calculated to be 32 kJ/mol. However, at 1000 °C and above, it shows a two-step parabolic oxidation kinetics, where the first stage (step I) was proposed to be dominated by the oxidation of surface TiC particles. After all the surface TiC particles are oxidized, the oxidation changes to the second stage (step II) that was controlled by the oxidation of $MoSi_2$. The activation energies were determined to be 130 kJ/mol and 141 kJ/mol for step I and step II, respectively. A dense cristobalite scale with TiO_2 in lath shapes on the top was observed after

oxidation at 1400 °C. The dense SiO_2 scale is a good barrier to oxygen diffusion at high-temperature, providing good high-temperature oxidation resistance for the composite.

References

1. K. VASUDEVAN and J. J. PETROVIC, *Mater. Sci. Eng.* **A155** (1995) 1.
2. P. J. MESCHTER and D. S. SCHWARTZ, *JOM* **41** (1989) 52.
3. J. SCHLICHTING, *High Temperature High Pressure* **10** (1978) 241.
4. R. M. AIKEN, *Scr. Metall. Mater.* **26** (1992) 1025.
5. K. ITO, T. YANO, T. NAKAMOTO, M. MORIWAKI, H. INUI and M. YAMAGUCHI, *Progress in Materials Science* **42** (1997) 193.
6. J. WOLFENSTINE, Y. L. JENG and E. J. LAVERNIA, *Mater. Sci. Eng.* **A189** (1994) 257.
7. J. I. LEE, N. L. HECHT and T. MAH, *J. Amer. Ceram. Soc.* **81** (1998) 421.
8. S. MALOY, A. H. HEUER, J. LEWANDOWSKI and J. PETROVIC, *ibid.* **74** (1991) 2704.
9. K. K. RICHARDSON and D. W. FREITAG, *Ceram. Eng. Sci. Proc.* **12** (1991) 1679.
10. R. GIBALA, A. K. GHOSH, D. C. VAN AKEN, D. J. SROLOVITZ, A. BASU, H. CHANG, D. P. MASON and W. YANG, *Mater. Sci. Eng.* **A155** (1992) 147.
11. J. M. YANG and S. M. JENG, *J. Mater. Res.* **6** (1991) 505.
12. J. M. YANG, W. KAI and S. M. JENG, *Scripta Metallurgica* **23** (1989) 1953.
13. J. SUBRAHMANYAM, R. M. RAO and G. SUNDARASARMA, *J. Mater. Res.* **10** (1995) 1226.
14. I. PHO, H. W. KING and S. D. GUPTA, *J. Can. Ceram. Soc.* **66** (1997) 56.
15. M. W. BARSOUM and T. EL-RAGHY, *J. Electrochem. Soc.* **144** (1997) 2508.
16. W. B. WHITE, S. M. JOHNSON and G. B. DANTZIG, *J. Chem. Phys.* **28** (1958) 751.
17. Q. ZHU, X. QIU and C. MA, *Computers & Applied Chemistry* **13** (1996) 91.
18. I. BARIN, F. SAUERT, E. SCHULTZE-RHONHOF and S. S. WANG, *Thermochemical Data of Pure Substance* (VC11, Weinheim, Federal Republic of Germany, 1993).
19. M. W. CHASE, JR., C. W. DAVIES, J. R. DOWNEY, JR., D. J. FRURIP, R. A. MCDONALD and A. N. SYVERUD, *JANAF Thermochemical Tables*, 3rd ed., *J. Phys. Chem. Ref. Data*, Vol. 14, Suppl. 1 (American Chemical Society, New York, 1985).
20. S. SHIMADA, *J. Mater. Sci.* **31** (1996) 673.
21. Q. ZHU, K. SHOBU, E. TANI, K. KISHI and S. UMEBAYASHI, *ibid.* **35** (2000) 863.
22. M. K. MEYER and M. AKINC, *J. Amer. Ceram. Soc.* **79** (1996) 938.
23. T. C. CHOU and T. G. NIEH, *J. Mater. Res.* **8** (1993) 1605.
24. P. J. MESCHTER, *Met. Trans.* **A23** (1992) 1763.
25. D. S. FOX, *J. Amer. Ceram. Soc.* **81** (1998) 945.
26. S. SHIMADA and M. KOZEKI, *J. Mater. Sci.* **29** (1992) 1869.
27. A. TAMPIERI and A. BELLOSI, *J. Amer. Ceram. Soc.* **75** (1992) 1688.
28. E. L. WILLIAMS, *ibid.* **48** (1965) 190.
29. F. J. NORTON, *Nature* **191** (1961) 701.
30. B. E. DEAL and A. S. GROVE, *J. Appl. Phys.* 36 (1965) 3370.
31. C. B. LIM, T. YANO and T. ISEKI, *J. Mater. Sci.* **24** (1989) 4144.

Received 8 February
and accepted 21 June 2000